AIAA 2013-2830

Nodal Points and the Nonlinear Stability of High-Order Methods for Unsteady Flow Problems on Tetrahedral Meshes

David M. Williams*, Antony Jameson†
Department of Aeronautics and Astronautics, Stanford University, Stanford, CA, 94305

High-order methods have the potential to efficiently generate accurate solutions to fluid dynamics problems of practical interest. However, high-order methods are less robust than lower-order methods, as they are less dissipative, making them more susceptible to spurious oscillations and aliasing driven instabilities that arise during simulations of nonlinear phenomena. An effective approach for addressing this issue comes from noting that, for nonlinear problems, the stability of high-order nodal methods is significantly effected by the locations of the nodal points. In fact, in 1D and 2D, it has been shown that placing the nodal points at the locations of quadrature points reduces aliasing errors and improves the robustness of high-order schemes. In this paper, the authors perform an investigation of a particular set of nodal points whose locations coincide with quadrature points. Analysis is performed in order to determine the conditioning of these points and their suitability for interpolation. Thereafter, numerical experiments are performed on several canonical 3D problems in order to show that this set of nodal points is effective in reducing aliasing errors and promoting nonlinear stability.

I. Introduction

High-order methods produce less numerical dissipation than their low-order counterparts (for which the order is ≤ 2), and as a result, are well-suited for simulating vortex-dominated flows[1]. In particular, high-order methods have been successfully employed to simulate flows over flapping wings[2,3], rotorcraft[4], turbine blades[5], and high-lift devices[6]. Despite their success in these settings, they have yet to be adopted by a wide community of fluid-dynamicists. High-order methods are not as robust or as intuitive as low-order methods, and thus have yet to gain wide acceptance in industry and academia.

Recently, a number of efforts have been focused on addressing the shortcomings of high-order methods. In particular, significant effort has gone toward improving the 'ease of implementation' associated with these methods. Initially, the most popular high-order methods, (the discontinuous Galerkin (DG) methods) made use of complex quadrature procedures and primarily employed modal representations of the solution in each element[7–9]. However, recently, nodal DG methods that make use of pre-integrated quadratures and primarily employ nodal representations of the solution have gained recognition. For further details, one may consult the book by Hesthaven and Warburton[10], which provides a review of these methods. Furthermore, other high-order nodal methods, including the Spectral Difference (SD)[11,12] method have risen in prominence. In addition, the Flux Reconstruction (FR) approach due to Huynh[13] has emerged as a single framework which unifies a number of well-known high-order methods including the nodal DG method along with several SD methods (at least for linear problems). Using this framework, Jameson[14] identified an SD scheme that was stable for linear advection in 1D and, thereafter Vincent, Castonguay, and Jameson[15] identified a class of energy-stable FR schemes referred to as the VCJH (Vincent-Castonguay-Jameson-Huynh) schemes. The VCJH schemes have been shown to be stable for linear advection-diffusion problems in multiple dimensions[16–18]. Thus, it can be said that the linear stability of the schemes has been well established.

*Ph.D. Candidate, Department of Aeronautics and Astronautics, Stanford University, AIAA Student Member
†Thomas V. Jones Professor of Engineering, Department of Aeronautics and Astronautics, Stanford University, AIAA Member

There are, however, concerns regarding the *nonlinear* stability of high-order nodal schemes, including the VCJH schemes. High-order nodal methods generally approximate the flux using a collocation projection of the flux onto the polynomial space of degree p. When the flux is highly nonlinear, this approach tends to introduce aliasing errors that have the potential to destabilize the solution [10], especially in the absence of the excess numerical dissipation that is often provided by 1st or 2nd-order methods. Recent efforts have been devoted towards choosing nodal sets that tend to reduce these aliasing errors. In particular, preliminary results in 1D and 2D indicate that choosing to locate the nodal points at the locations of quadrature points tends to dampen aliasing driven instabilities [19,20]. This paper extends these efforts to 3D and attempts to find nodal sets that reduce aliasing errors on tetrahedral elements. In particular, the majority of attention is focused on the recently discovered quadrature points due to Shunn, Ham, and Williams [18,21]. These points, along with more traditional sets of nodal points due to [10,22] are evaluated and their suitability for nonlinear problems is assessed.

The structure of the paper is as follows. In section II, a high-order nodal method (the FR method) for treating a nonlinear advection-diffusion problem will be presented. Thereafter, in section III, the link between the locations of the nodal points and the nonlinear stability of high-order nodal methods (and in particular the energy stable FR methods (VCJH schemes)) will be examined. Next, in section IV, the conditioning of various nodal sets will be examined. Finally, section V will present the results of numerical experiments comparing the performance of nodal sets on a succession of nonlinear advection-diffusion problems.

II. Flux Reconstruction Schemes for Nonlinear Advection-Diffusion

The particulars of high-order nodal schemes (such as the FR schemes) can be best understood by examining the application of these schemes to a model problem. Towards this end, consider the application of an FR scheme to the following nonlinear advection-diffusion equation

$$\frac{\partial u}{\partial t} + \nabla \cdot \mathbf{f}\left(u, \nabla u\right) = 0, \tag{1}$$

where $u\left(\mathbf{x}, t\right)$ is a scalar solution, $\mathbf{f} = \mathbf{f}\left(u, \nabla u\right)$ is a vector-valued flux, t is time, $\mathbf{x} = (x, y, z) \equiv (x_1, x_2, x_3)$ is a vector of spatial coordinates defined on the domain $\mathbf{\Omega}$ with boundary $\mathbf{\Gamma}$, and $\nabla = \left(\frac{\partial}{\partial x}, \frac{\partial}{\partial y}, \frac{\partial}{\partial z}\right)$ is a gradient operator. In general, upon expanding the second term on the left hand side of equation (1), one obtains second derivatives of the solution u. These second derivatives are difficult to discretize, and therefore equation (1) is usually rewritten as a system of two equations each of which contain first derivatives. In order to transform equation (1) into a system of two first-order equations, one may introduce a new variable $\mathbf{q}$ in place of ∇u as follows

$$\frac{\partial u}{\partial t} + \nabla \cdot \mathbf{f}\left(u, \mathbf{q}\right) = 0, \tag{2}$$

$$\mathbf{q} - \nabla u = 0. \tag{3}$$

In what follows, the variable $\mathbf{q}$ will be referred to as the 'auxiliary variable.' Now, having rewritten the advection-diffusion equation in a more convenient form (equations (2) and (3)), one may attempt to find an approximate solution on the domain $\mathbf{\Omega}$. Towards this end, one may divide the domain $\mathbf{\Omega}$ into N non-overlapping, conforming, straight-sided tetrahedron elements $\mathbf{\Omega}_k$ as follows

$$\mathbf{\Omega} = \bigcup_{k=1}^{N} \mathbf{\Omega}_k, \tag{4}$$

$$\mathbf{\Omega}_i \cap \mathbf{\Omega}_j = \emptyset \qquad \forall i \neq j. \tag{5}$$

One may now obtain approximate formulations of equations (2) and (3) on the k^{th} element $\mathbf{\Omega}_k$. Towards this end, consider defining u_k^D, a degree p polynomial approximation to the solution that takes the following form

$$u_k^D = \sum_{i=1}^{N_p} \left(u_k^D\right)^i \ell_i\left(\mathbf{x}\right), \tag{6}$$

where each $\left(u_k^D\right)^i$ is the value of the solution at each nodal solution point $\mathbf{x}_i$, each $\ell_i(\mathbf{x})$ is a nodal basis function which assumes the value of 1 at each nodal solution point $\mathbf{x}_i$ and the value of 0 at all other nodal solution points, and N_p is the number of nodal solution points defined such that $N_p \equiv (p+1)(p+2)(p+3)/3!$. Note that the superscript D on u_k^D refers to the fact that (in general) u_k^D is discontinuous at the boundary between neighboring elements $\mathbf{\Omega}_k$ and $\mathbf{\Omega}_{k+1}$.

An approximate formulation of the auxiliary variable can be constructed in a similar manner. In particular, each component of the auxiliary variable can be represented using a polynomial of degree p as follows

$$\begin{aligned} \mathbf{q}_k^D &= \left(q_{x_k}^D, q_{y_k}^D, q_{z_k}^D\right), \\ q_{m_k}^D &= \sum_{i=1}^{N_p} (q_{m_k}^D)^i \, \ell_i(\mathbf{x}) \quad \forall \quad m = 1,2,3, \end{aligned} \tag{7}$$

where each $(q_{m_k}^D)^i$ is the value of the mth component of the auxiliary variable at each nodal solution point $\mathbf{x}_i$. Finally, one may construct an approximate formulation of the flux via a 'collocation projection' at the N_p nodal solution points as follows

$$\begin{aligned} \mathbf{f}_k^D &= \left(f_{x_k}^D, f_{y_k}^D, f_{z_k}^D\right), \\ f_{m_k}^D &= \sum_{i=1}^{N_p} (f_{m_k}^D)^i \, \ell_i(\mathbf{x}) \quad \forall \quad m = 1,2,3, \end{aligned} \tag{8}$$

where each $(f_{m_k}^D)^i$ is the value of the mth component of the flux at each nodal solution point $\mathbf{x}_i$ computed from the value of the solution $\left(u_k^D\right)^i$ and the auxiliary variable $\left(\mathbf{q}_k^D\right)^i$ at each nodal solution point. The form of the flux in equation (8) is referred to as a 'collocation projection form' because it projects the flux, which is usually nonlinear and of degree $> p$, unto a polynomial basis of degree p.

One may now substitute the approximate quantities u_k^D, $\mathbf{q}_k^D$, and $\mathbf{f}_k^D$ into equations (2) and (3) in place of u, $\mathbf{q}$, and $\mathbf{f}$ in order to obtain the following

$$\frac{\partial u_k^D}{\partial t} + \nabla \cdot \mathbf{f}_k^D = 0, \tag{9}$$

$$\mathbf{q}_k^D - \nabla u_k^D = 0. \tag{10}$$

In their current form, equations (9) and (10) do not represent a valid numerical scheme, as the solution u_k^D is influenced only by information that is local to the k^{th} element. In order to resolve this problem, the FR approach couples the approximate solution u_k^D in the k^{th} element to the solutions in neighboring elements by replacing the discontinuous flux $\mathbf{f}_k^D$ in equation (9) with a continuous flux $\mathbf{f}_k$ of degree $p+1$. The flux $\mathbf{f}_k$ is continuous in the sense that the normal components $\mathbf{f}_k \cdot \mathbf{n}$ and $\mathbf{f}_{k+1} \cdot \mathbf{n}$ are required to be equal to one another on the boundary between $\mathbf{\Omega}_k$ and $\mathbf{\Omega}_{k+1}$. Furthermore, the FR approach replaces the discontinuous solution u_k^D in equation (10) with a continuous solution u_k of degree $p+1$, where u_k and u_{k+1} are required to be equal to one another on the boundary between $\mathbf{\Omega}_k$ and $\mathbf{\Omega}_{k+1}$. The resulting FR formulation of equations (9) and (10) becomes

$$\frac{\partial u_k^D}{\partial t} + \nabla \cdot \mathbf{f}_k = 0, \tag{11}$$

$$\mathbf{q}_k^D - \nabla u_k = 0. \tag{12}$$

The continuous flux $\mathbf{f}_k$ is constructed from the sum of the degree p discontinuous flux $\mathbf{f}_k^D$ and a degree $p+1$ flux correction $\mathbf{f}_k^C$. Similarly, the continuous solution u_k is constructed from the sum of the degree p discontinuous solution u_k^D and a degree $p+1$ solution correction u_k^C. As a result, equations (11) and (12) can be rewritten as follows

$$\frac{\partial u_k^D}{\partial t} + \nabla \cdot \mathbf{f}_k^D + \nabla \cdot \mathbf{f}_k^C = 0, \tag{13}$$

$$\mathbf{q}_k^D - \nabla u_k^D - \nabla u_k^C = 0. \tag{14}$$

Prior to solving equations (13) and (14), it is convenient to first transform them from the physical element $\mathbf{\Omega}_k$ to the reference (or standard) tetrahedral element $\mathbf{\Omega}_S$. The reference element and an example of the nodal solution points ($\hat{\mathbf{x}}_i$) that reside in the interior of the reference element are shown in Figure (1).

A mapping $\mathbf{\Theta}_k$ between the physical coordinates $\mathbf{x}$ in $\mathbf{\Omega}_k$ and the reference coordinates $\hat{\mathbf{x}} = (\hat{x}, \hat{y}, \hat{z})$ in $\mathbf{\Omega}_S$ can be constructed as follows

$$\mathbf{x} = \mathbf{\Theta}_k\left(\hat{\mathbf{x}}\right) = -\frac{\hat{x}+\hat{y}+\hat{z}+1}{2}\mathbf{v}_{1,k} + \frac{\hat{x}+1}{2}\mathbf{v}_{2,k} + \frac{\hat{y}+1}{2}\mathbf{v}_{3,k} + \frac{\hat{z}+1}{2}\mathbf{v}_{4,k}, \tag{15}$$

where $\mathbf{v}_{1,k}$, $\mathbf{v}_{2,k}$, $\mathbf{v}_{3,k}$, and $\mathbf{v}_{4,k}$ are the vertices of $\mathbf{\Omega}_k$. Once the mapping is established, it is possible to transform u_k^D, $\mathbf{f}_k^D$, $\mathbf{f}_k^C$, $\mathbf{q}_k^D$, and u_k^C that reside in $\mathbf{\Omega}_k$ into $\hat{u}^D$, $\hat{\mathbf{f}}^D$, $\hat{\mathbf{f}}^C$, $\hat{\mathbf{q}}^D$, and $\hat{u}^C$ that reside in $\mathbf{\Omega}_S$ via the following transformations due to Viviand[23] and Vinokur[24]

$$\hat{u}^D = J_k u_k^D(\mathbf{\Theta}_k(\hat{\mathbf{x}}), t), \qquad \hat{u}^C = J_k u_k^C(\mathbf{\Theta}_k(\hat{\mathbf{x}}), t), \tag{16}$$

$$\hat{\mathbf{f}}^D = \begin{bmatrix}\hat{f}^D \\ \hat{g}^D\end{bmatrix} = J_k\,\mathbf{J}_k^{-1}\,\mathbf{f}_k^D, \qquad \hat{\mathbf{f}}^C = \begin{bmatrix}\hat{f}^C \\ \hat{g}^C\end{bmatrix} = J_k\,\mathbf{J}_k^{-1}\,\mathbf{f}_k^C, \qquad \hat{\mathbf{q}}^D = \begin{bmatrix}\hat{q}_{\hat{x}}^D \\ \hat{q}_{\hat{y}}^D\end{bmatrix} = \hat{\nabla}\hat{u} = J_k\,\mathbf{J}_k^T\,\mathbf{q}_k^D, \tag{17}$$

where

$$\mathbf{f}_k^D = \begin{bmatrix}f_k^D \\ g_k^D\end{bmatrix}, \qquad \mathbf{f}_k^C = \begin{bmatrix}f_k^C \\ g_k^C\end{bmatrix}, \qquad \mathbf{q}_k^D = \begin{bmatrix}q_{x_k}^D \\ q_{y_k}^D\end{bmatrix} = \nabla u_k, \tag{18}$$

and

$$\hat{\nabla} = \begin{bmatrix}\frac{\partial}{\partial \hat{x}} \\ \frac{\partial}{\partial \hat{y}}\end{bmatrix}, \qquad \mathbf{J}_k = \begin{bmatrix}\frac{\partial x}{\partial \hat{x}} & \frac{\partial x}{\partial \hat{y}} \\ \frac{\partial y}{\partial \hat{x}} & \frac{\partial y}{\partial \hat{y}}\end{bmatrix}, \qquad J_k = \det(\mathbf{J}_k). \tag{19}$$

Using these transformations, equations (13) and (14) can be reformulated as follows

$$\frac{\partial \hat{u}^D}{\partial t} + \hat{\nabla}\cdot\hat{\mathbf{f}}^D + \hat{\nabla}\cdot\hat{\mathbf{f}}^C = 0, \tag{20}$$

$$\hat{\mathbf{q}}^D - \hat{\nabla}\hat{u}^D - \hat{\nabla}\hat{u}^C = 0, \tag{21}$$

where

$$\hat{u}^D = \sum_{i=1}^{N_p}\left(\hat{u}^D\right)^i \hat{\ell}_i\left(\hat{\mathbf{x}}\right), \tag{22}$$

$$\hat{\mathbf{q}}^D = \left(\hat{q}_{\hat{x}}^D, \hat{q}_{\hat{y}}^D, \hat{q}_{\hat{z}}^D\right),$$

$$\hat{q}_m^D = \sum_{i=1}^{N_p}(\hat{q}_m^D)^i\,\hat{\ell}_i\left(\hat{\mathbf{x}}\right) \quad \forall \quad m = \hat{1}, \hat{2}, \hat{3}, \tag{23}$$

$$\hat{\mathbf{f}}^D = \left(\hat{f}_{\hat{x}}^D, \hat{f}_{\hat{y}}^D, \hat{f}_{\hat{z}}^D\right),$$

$$\hat{f}_m^D = \sum_{i=1}^{N_p}(\hat{f}_m^D)^i\,\hat{\ell}_i\left(\hat{\mathbf{x}}\right) \quad \forall \quad m = \hat{1}, \hat{2}, \hat{3}, \tag{24}$$

and where $\hat{\mathbf{f}}^C$ and $\hat{u}^C$ can be defined via several different approaches[18,25,26]. One such approach due to Williams and Jameson[18] utilizes the following expressions for computing $\hat{\nabla}\cdot\hat{\mathbf{f}}^C$ and $\hat{\nabla}\hat{u}^C$

$$\hat{\nabla}\cdot\hat{\mathbf{f}}^C = \sum_{f=1}^{4}\sum_{l=1}^{N_{fp}}\left(\left(\hat{\mathbf{f}}_{f,l}^{\star} - \hat{\mathbf{f}}_{f,l}^D\right)\cdot\hat{\mathbf{n}}_{f,l}\right)\phi_{f,l}, \tag{25}$$

$$\hat{\nabla}\hat{u}^C = \sum_{f=1}^{4}\sum_{l=1}^{N_{fp}}\left(\hat{u}_{f,l}^{\star} - \hat{u}_{f,l}^D\right)\hat{\mathbf{n}}_{f,l}\,\psi_{f,l}, \tag{26}$$

where N_{fp} is the number of nodal flux points located on each of the $f = 1, \ldots, 4$ faces of the reference tetrahedron (where an example of the $N_{fp} \equiv (p+1)(p+2)/2!$ points on each face is shown in Figure (2)), $\hat{\mathbf{f}}^{\star}_{f,l}$ is the value of the numerical flux at nodal flux point l on face f (denoted by $\hat{\mathbf{x}}_{f,l}$), $\hat{\mathbf{f}}^{D}_{f,l}$ is the value of the discontinuous flux at $\hat{\mathbf{x}}_{f,l}$, $\hat{\mathbf{n}}_{f,l}$ is the value of the normal at $\hat{\mathbf{x}}_{f,l}$, $\hat{u}^{\star}_{f,l}$ is the value of the numerical solution at $\hat{\mathbf{x}}_{f,l}$, $\hat{u}^{D}_{f,l}$ is the value of the discontinuous solution at $\hat{\mathbf{x}}_{f,l}$, and $\phi_{f,l}$ and $\psi_{f,l}$ are the VCJH correction fields or 'lifting operators' associated with $\hat{\mathbf{x}}_{f,l}$. The purpose of the correction fields is to take information at the boundaries of the element and propagate it into the interior of the element. Note that this approach for constructing $\hat{\nabla} \cdot \hat{\mathbf{f}}^{C}$ and $\hat{\nabla}\hat{u}^{C}$ is a variant of the VCJH approaches in 1D and 2D that were referred to previously[15,16]. An important characteristic of this approach is that it recovers an infinite range of energy stable FR schemes ('VCJH schemes') that are provably stable for linear advection-diffusion problems on tetrahedral elements[18].

III. Nonlinear Stability of Flux Reconstruction Schemes

Although the linear stability of certain FR schemes (in particular the VCJH schemes) has been established, the nonlinear stability of these schemes is still under review. Most recently, the nonlinear stability of the VCJH schemes was evaluated by Williams[18] for the following nonlinear advection-diffusion problem

$$\frac{\partial u}{\partial t} + \nabla \cdot \left(\mathbf{f}_{adv}\left(u\right) + \mathbf{f}_{dif}\left(u, \mathbf{q}\right) \right) = 0, \tag{27}$$

$$\mathbf{q} - \nabla u = 0, \tag{28}$$

where $\mathbf{f}_{adv}$ and $\mathbf{f}_{dif}$ are nonlinear advective and diffusive fluxes, respectively, and where in particular

$$\mathbf{f}_{dif}\left(u, \mathbf{q}\right) = -b\left(u\right)\mathbf{q}. \tag{29}$$

Here, $b\left(u\right)$ is a non-negative, nonlinear diffusivity coefficient. In[18], it was shown that if a VCJH scheme is applied to this nonlinear advection-diffusion problem, the time rate of change of a matrix-based norm of the approximate solution is governed by the following equation

$$\frac{1}{2}\sum_{k=1}^{N}\left(\frac{\mathrm{d}}{\mathrm{d}t}\|\mathbf{U}_k\|^2_{\widetilde{\mathbf{M}}}\right) + \sum_{k=1}^{N}\left(\mathbf{Q}_k^T \mathcal{B}_k \widetilde{\mathcal{M}}^k\, \mathbf{Q}_k\right) = \Xi_{interfaces} + \Xi_{alias}, \tag{30}$$

where $\mathbf{U}_k = \left[(u_k^D)^1 \ \ldots \ (u_k^D)^{N_p}\right]^T$ is a vector containing the solution values, $\mathbf{Q}_k = \left[\mathbf{Q}_{x_k}\mathbf{Q}_{y_k}\mathbf{Q}_{z_k}\right]^T = \left[\mathbf{Q}_{1_k}\mathbf{Q}_{2_k}\mathbf{Q}_{3_k}\right]^T$ (where $\mathbf{Q}_{m_k} = \left[(q_{m_k}^D)^1 \ \ldots \ (q_{m_k}^D)^{N_p}\right]^T$) is a vector containing the auxiliary variable values, $\widetilde{\mathbf{M}}^k$ and $\widetilde{\mathcal{M}}^k$ are symmetric, positive-definite, augmented mass matrices,

$$\|\mathbf{U}_k\|_{\widetilde{\mathbf{M}}} = \left(\mathbf{U}_k^T\, \widetilde{\mathbf{M}}^k\, \mathbf{U}_k\right)^{1/2} \tag{31}$$

is a matrix-based norm, $\mathcal{B}_k = \mathrm{diag}\left[\mathbf{B}_k\, \mathbf{B}_k\, \mathbf{B}_k\right]$ (where $\mathbf{B}_k = \mathrm{diag}\left[b\left((u_k^D)^1\right) \ \ldots b\left((u_k^D)^{N_p}\right)\right]$) is a matrix of nonlinear diffusion coefficients, $\Xi_{interfaces}$ is a summation of interface contributions, and Ξ_{alias} is a summation of aliasing errors introduced by the collocation projection of the flux. The sign of Ξ_{alias} is generally unknown, and as a result, it may cause the time rate of change of the solution to become positive and for the scheme to become unstable. Therefore, in order to promote stability of the scheme, it is necessary to minimize or eliminate this term. To see how this can be accomplished, it is useful to examine the following precise definition of the aliasing error term

$$\Xi_{alias} \equiv \sum_{k=1}^{N}\left(\varepsilon_{\mathbf{\Omega}_k} + \varepsilon_{\mathbf{\Gamma}_k}\right), \tag{32}$$

where

$$\varepsilon_{\mathbf{\Omega}_k} \equiv \int_{\mathbf{\Omega}_k} \nabla u_k^D \cdot \left(\mathbf{f}^D_{k,\,adv} - \mathbf{f}_{adv}\left(u_k^D\right)\right) d\mathbf{\Omega}_k, \tag{33}$$

$$\varepsilon_{\mathbf{\Gamma}_k} \equiv \int_{\mathbf{\Gamma}_k} \left[\left(u_k^D - u^{\star}\right)\left(\mathbf{f}^D_{k,\,dif} - \mathbf{f}_{dif}\left(u_k^D, \mathbf{q}_k^D\right)\right)\right] \cdot \mathbf{n}\, d\mathbf{\Gamma}_k. \tag{34}$$

Here, $\varepsilon_{\mathbf{\Omega}_k}$ and $\varepsilon_{\mathbf{\Gamma}_k}$ are measures of the effective 'distances' between the exact flux functions ($\mathbf{f}_{adv}\left(u_k^D\right)$ and $\mathbf{f}_{dif}\left(u_k^D, \mathbf{q}_k^D\right)$) and the approximate fluxes ($\mathbf{f}_{k,\,adv}^D$ and $\mathbf{f}_{k,\,dif}^D$). It turns out that $\varepsilon_{\mathbf{\Omega}_k}$ and $\varepsilon_{\mathbf{\Gamma}_k}$ can be eliminated if exact 'L2 projections' are utilized to construct the fluxes $\mathbf{f}_{k,\,adv}^D$ and $\mathbf{f}_{k,\,dif}^D$ on $\mathbf{\Omega}_k$ and $\mathbf{\Gamma}_k$, respectively. This will be shown via a brief examination of these L2 projections.

Consider the exact L2 projection of a flux $\mathbf{f}_k^D$ on $\mathbf{\Omega}_k$ which can be defined such that

$$\forall i \quad \int_{\mathbf{\Omega}_k} \left(\mathbf{f}_k^D - \mathbf{f}\left(u_k^D\right)\right) L_{k,i}^{3D}\, d\mathbf{\Omega}_k = 0, \tag{35}$$

where each $L_{k,i}^{3D} = L_{k,i}^{3D}\left(\mathbf{x}\right)$ is a member of a 3D orthonormal polynomial basis of degree $p-1$ on $\mathbf{\Omega}_k$. Furthermore, the exact L2 projection of a flux $\mathbf{f}_k^D$ on $\mathbf{\Gamma}_k$ can be defined such that for each of the $f = 1, \ldots, 4$ faces of the element boundary

$$\forall l \quad \int_{\mathbf{\Gamma}_f} \left(\mathbf{f}_k^D - \mathbf{f}\left(u_k^D\right)\right) \cdot \mathbf{n}_f\, L_{k,f,l}^{2D}\, d\mathbf{\Gamma}_f = 0, \tag{36}$$

where each $L_{k,f,l}^{2D} = L_{k,f,l}^{2D}\left(\mathbf{x}\right)$ is a member of a 2D orthonormal polynomial basis of degree p on $\mathbf{\Gamma}_f$.

Setting equations (35) and (36) aside for the moment, consider representing ∇u_k^D on $\mathbf{\Omega}_k$ and $\left(u_k^D - u^\star\right)$ on $\mathbf{\Gamma}_f$ in terms of the orthonormal basis functions $L_{k,i}^{3D}$ and $L_{k,f,l}^{2D}$ as follows

$$\left(\nabla u_k^D\right)_m = \sum_{i=1}^{\widetilde{N}_p} \zeta_{k,i,m}\, L_{k,i}^{3D}\left(\mathbf{x}\right), \qquad \text{for} \quad m = 1, 2, 3, \tag{37}$$

$$\left(u_k^D - u^\star\right)_f = \sum_{l=1}^{N_{fp}} \varphi_{k,f,l}\, L_{k,f,l}^{2D}\left(\mathbf{x}\right), \tag{38}$$

where $\zeta_{k,i,m}$ and $\varphi_{k,f,l}$ are constant coefficients, and $\widetilde{N}_p$ is the number of points required to define a polynomial of degree $p-1$ in 3D, i.e. $\widetilde{N}_p \equiv p\left(p+1\right)\left(p+2\right)/3!$. Upon multiplying equation (35) by each coefficient $\zeta_{k,i,m}$, substituting $\mathbf{f}_{adv}$ in place of $\mathbf{f}$, and summing the result over m and i, one obtains

$$\int_{\mathbf{\Omega}_k} \nabla u_k^D \cdot \left(\mathbf{f}_{k,\,adv}^D - \mathbf{f}_{adv}\left(u_k^D\right)\right)\, d\mathbf{\Omega}_k = \varepsilon_{\mathbf{\Omega}_k} = 0. \tag{39}$$

Similarly, on multiplying equation (36) by each coefficient $\varphi_{k,f,l}$, substituting $\mathbf{f}_{dif}$ in place of $\mathbf{f}$, and summing the result over l and f, one obtains

$$\int_{\mathbf{\Gamma}_k} \left[\left(u_k^D - u^\star\right)\left(\mathbf{f}_{k,\,dif}^D - \mathbf{f}_{dif}\left(u_k^D, \mathbf{q}_k^D\right)\right)\right] \cdot \mathbf{n}\, d\mathbf{\Gamma}_k = \varepsilon_{\mathbf{\Gamma}_k} = 0. \tag{40}$$

From equations (39), (40), and (32), it immediately follows that $\Xi_{alias} = 0$.

It is important to note, that one is frequently unable to compute exact L2 projections of high dimensional or infinite dimensional nonlinear fluxes $\mathbf{f}_{adv}\left(u_k^D\right)$ and $\mathbf{f}_{dif}\left(u_k^D, \mathbf{q}_k^D\right)$ in problems of practical interest. However, if numerical quadrature rules of sufficiently high-order are employed in equations (35) and (36), the L2 projections can ensure that Ξ_{alias} is of the order of machine zero. Nevertheless, in this case, the L2 projection procedures will be substantially more expensive, from a computational standpoint, than the collocation projection utilized previously to define $\mathbf{f}_k^D$ (in equation (8)).

It turns out that one may utilize collocation projection procedures to form the fluxes while simultaneously reducing aliasing errors, if the nodal solution points $\mathbf{x}_i$ and nodal flux points $\mathbf{x}_{f,l}$ are placed at the locations of quadrature points. This can be shown via further examination of the aliasing errors $\varepsilon_{\mathbf{\Omega}_k}$ and $\varepsilon_{\mathbf{\Gamma}_k}$. Towards this end, consider transforming $\varepsilon_{\mathbf{\Omega}_k}$ and $\varepsilon_{\mathbf{\Gamma}_k}$ from the physical space to the reference space as follows

$$\varepsilon_{\mathbf{\Omega}_k} = \frac{\hat{\varepsilon}_{\mathbf{\Omega}_S}}{J_k} = \frac{1}{J_k}\int_{\mathbf{\Omega}_S} \hat{\nabla}\hat{u}^D \cdot \left(\hat{\mathbf{f}}_{adv}^D - \hat{\mathbf{f}}_{adv}\left(\hat{u}^D\right)\right)\, d\mathbf{\Omega}_S, \tag{41}$$

$$\varepsilon_{\mathbf{\Gamma}_k} = \frac{\hat{\varepsilon}_{\mathbf{\Gamma}_S}}{J_k} = \frac{1}{J_k}\int_{\mathbf{\Gamma}_S} \left[\left(\hat{u}^D - \hat{u}^\star\right)\left(\hat{\mathbf{f}}_{dif}^D - \hat{\mathbf{f}}_{dif}\left(\hat{u}^D, \hat{\mathbf{q}}^D\right)\right)\right] \cdot \hat{\mathbf{n}}\, d\mathbf{\Gamma}_S, \tag{42}$$

where $\hat{\varepsilon}_{\mathbf{\Omega}_S}$ and $\hat{\varepsilon}_{\mathbf{\Gamma}_S}$ are measures of the aliasing errors in the reference space. (Note that the transformation to reference space has been performed in order to simplify the subsequent analysis).

Next, one may define $\hat{\nabla}\hat{u}^D$ in equation (41) and $\left(\hat{u}^D - \hat{u}^\star\right)$ in equation (42) as follows

$$\left(\hat{\nabla}\hat{u}^D\right)_m = \sum_{i=1}^{\widetilde{N}_p} \hat{\zeta}_{i,m}\, L_i^{3D}\left(\hat{\mathbf{x}}\right), \qquad \text{for} \quad m = \hat{1}, \hat{2}, \hat{3}, \tag{43}$$

$$\left(\hat{u}^D - \hat{u}^\star\right)_f = \sum_{l=1}^{N_{fp}} \hat{\varphi}_{f,l}\, L_{f,l}^{2D}\left(\hat{\mathbf{x}}\right), \tag{44}$$

where $\hat{\zeta}_{i,m}$ and $\hat{\varphi}_{f,l}$ are constant coefficients, $L_i^{3D} = L_i^{3D}\left(\hat{\mathbf{x}}\right)$ is a member of the 3D orthonormal polynomial basis of degree $p-1$ inside the reference element, and $L_{f,l}^{2D} = L_{f,l}^{2D}\left(\hat{\mathbf{x}}\right)$ is a member of the 2D orthonormal polynomial basis of degree p on face f of the reference element. Upon substituting equations (43) and (44) into the expressions for $\hat{\varepsilon}_{\mathbf{\Omega}_S}$ and $\hat{\varepsilon}_{\mathbf{\Gamma}_S}$ in equations (41) and (42), one obtains

$$\hat{\varepsilon}_{\mathbf{\Omega}_S} = \sum_{m=\hat{1}}^{\hat{3}} \sum_{i=1}^{\widetilde{N}_p} \hat{\zeta}_{i,m} \int_{\mathbf{\Omega}_S} \left(\hat{f}_{m,\,adv}^D - \hat{f}_{m,\,adv}\left(\hat{u}^D\right)\right) L_i^{3D}\, d\mathbf{\Omega}_S, \tag{45}$$

$$\begin{aligned}\hat{\varepsilon}_{\mathbf{\Gamma}_S} &= \sum_{f=1}^{4} \sum_{l=1}^{N_{fp}} \hat{\varphi}_{f,l} \int_{\mathbf{\Gamma}_f} \left[\left(\hat{\mathbf{f}}_{dif}^D - \hat{\mathbf{f}}_{dif}\left(\hat{u}^D, \hat{\mathbf{q}}^D\right)\right) \cdot \hat{\mathbf{n}}_f\right] L_{f,l}^{2D}\, d\mathbf{\Gamma}_f \\ &= \sum_{m=\hat{1}}^{\hat{3}} \sum_{f=1}^{4} \sum_{l=1}^{N_{fp}} \hat{\varphi}_{f,l}\, \hat{n}_{f,m} \int_{\mathbf{\Gamma}_f} \left(\hat{f}_{m,\,f,\,dif}^D - \hat{f}_{m,\,dif}\left(\hat{u}_f^D, \hat{\mathbf{q}}_f^D\right)\right) L_{f,l}^{2D}\, d\mathbf{\Gamma}_f,\end{aligned} \tag{46}$$

or equivalently,

$$\hat{\varepsilon}_{\mathbf{\Omega}_S} = \sum_{m=\hat{1}}^{\hat{3}} \sum_{i=1}^{\widetilde{N}_p} \hat{\zeta}_{i,m} \left(\hat{\varepsilon}_{\mathbf{\Omega}_S}\right)_{i,m}, \tag{47}$$

$$\hat{\varepsilon}_{\mathbf{\Gamma}_S} = \sum_{m=\hat{1}}^{\hat{3}} \sum_{f=1}^{4} \sum_{l=1}^{N_{fp}} \hat{\varphi}_{f,l}\, \hat{n}_{f,m} \left(\hat{\varepsilon}_{\mathbf{\Gamma}_S}\right)_{f,l,m}, \tag{48}$$

where

$$\left(\hat{\varepsilon}_{\mathbf{\Omega}_S}\right)_{i,m} = \int_{\mathbf{\Omega}_S} \left(\hat{f}_{m,\,adv}^D - \hat{f}_{m,\,adv}\left(\hat{u}^D\right)\right) L_i^{3D}\, d\mathbf{\Omega}_S, \tag{49}$$

$$\left(\hat{\varepsilon}_{\mathbf{\Gamma}_S}\right)_{f,l,m} = \int_{\mathbf{\Gamma}_f} \left(\hat{f}_{m,\,f,\,dif}^D - \hat{f}_{m,\,dif}\left(\hat{u}_f^D, \hat{\mathbf{q}}_f^D\right)\right) L_{f,l}^{2D}\, d\mathbf{\Gamma}_f. \tag{50}$$

It should be noted that equations (49) and (50) are analogous to equations (35) and (36) that define the L2 projections in physical space. In fact, equations (49) and (50) simply define the component-wise L2 projections of the advective and diffusive fluxes in reference space. Thus, if exact L2 projections of the fluxes are performed then $\left(\hat{\varepsilon}_{\mathbf{\Omega}_S}\right)_{i,m}$ and $\left(\hat{\varepsilon}_{\mathbf{\Gamma}_S}\right)_{f,l,m}$ vanish as expected. However, for collocation projections of the flux, this is not necessarily the case. In order to illustrate this point, one may consider forming collocation projections of the fluxes as follows

$$\hat{f}_{m,\,adv}^D = \sum_{j=1}^{N_p} \hat{f}_{m,\,adv}\left(\left(\hat{u}^D\right)^j\right) \ell_j^{3D}\left(\hat{\mathbf{x}}\right) \qquad = \sum_{j=1}^{N_p} \left(\hat{f}_{m,\,adv}^D\right)^j \hat{\ell}_j^{3D}, \tag{51}$$

$$\hat{f}_{m,\,f,\,dif}^D = \sum_{r=1}^{N_{fp}} \hat{f}_{m,\,dif}\left(\left(\hat{u}_f^D\right)^r, \left(\hat{\mathbf{q}}_f^D\right)^r\right) \ell_{f,r}^{2D}\left(\hat{\mathbf{x}}\right) = \sum_{r=1}^{N_{fp}} \left(\hat{f}_{m,\,f,\,dif}^D\right)^r \hat{\ell}_{f,r}^{2D}, \tag{52}$$

where $\hat{\ell}_j^{3D}$ is the 3D nodal polynomial of degree p that assumes the value of 1 at nodal solution point j and the value of zero at all neighboring nodal solution points, $\hat{\ell}_{f,r}^{2D}$ is the 2D nodal polynomial of degree p that assumes the value

of 1 at nodal flux point f, r and the value of zero at all neighboring nodal flux points, and where $\left(\hat{f}^D_{m,\,adv}\right)^j$ and $\left(\hat{f}^D_{m,f,\,dif}\right)^r$ are the mth components of the pointwise values of the advective and diffusive fluxes in reference space ($\left(\hat{\mathbf{f}}^D_{adv}\right)^j$ and $\left(\hat{\mathbf{f}}^D_{f,\,dif}\right)^r$) that are the reference space equivalents of the pointwise values of the fluxes in physical space ($\left(\mathbf{f}^D_{k,\,adv}\right)^j = \mathbf{f}_{k,\,adv}\left(\left(u^D_k\right)^j\right)$ and $\left(\mathbf{f}^D_{k,f,\,dif}\right)^r = \mathbf{f}_{k,\,dif}\left(\left(u^D_f\right)^r, \left(\mathbf{q}^D_f\right)^r\right)$). Upon substituting equations (51) and (52) into equations (49) and (50), one obtains

$$\left(\hat{\varepsilon}_{\mathbf{\Omega}_S}\right)_{i,m} = \sum_{j=1}^{N_p} \left(\hat{f}^D_{m,\,adv}\right)^j \int_{\mathbf{\Omega}_S} \hat{\ell}^{3D}_j L^{3D}_i \; \mathbf{\Omega}_S - \int_{\mathbf{\Omega}_S} \hat{f}_{m,\,adv}\left(\hat{u}^D\right) L^{3D}_i \; d\mathbf{\Omega}_S, \tag{53}$$

$$\left(\hat{\varepsilon}_{\mathbf{\Gamma}_S}\right)_{f,l,m} = \sum_{r=1}^{N_{fp}} \left(\hat{f}^D_{m,f,\,dif}\right)^r \int_{\mathbf{\Gamma}_f} \hat{\ell}^{2D}_{f,r} L^{2D}_{f,l} \; d\mathbf{\Gamma}_f - \int_{\mathbf{\Gamma}_f} \hat{f}_{m,\,dif}\left(\hat{u}^D_f, \hat{\mathbf{q}}^D_f\right) L^{2D}_{f,l} \; d\mathbf{\Gamma}_f. \tag{54}$$

The terms $\hat{\ell}^{3D}_j L^{3D}_i$ and $\hat{\ell}^{2D}_{f,r} L^{2D}_{f,l}$ that appear in equations (53) and (54) are polynomials of degree $2p-1$ in 3D and degree $2p$ in 2D, respectively. Thus, the integrals of these terms can be computed exactly via quadrature rules of degree $2p-1$ in 3D and degree $2p$ in 2D. More generally, a 3D quadrature rule (or equivalently a cubature rule) of arbitrary degree can approximate the integral of $\hat{\ell}^{3D}_j L^{3D}_i$ on $\mathbf{\Omega}_S$ as follows

$$\int_{\mathbf{\Omega}_S} \hat{\ell}^{3D}_j L^{3D}_i \; \mathbf{\Omega}_S = \sum_{n=1}^{N^{3D}_q} w_n \, \hat{\ell}^{3D}_j\left(\varsigma_n\right) L^{3D}_i\left(\varsigma_n\right) + e^{3D}_q, \tag{55}$$

where N^{3D}_q is the number of quadrature points, ς_n's are the point locations, w_n's are the weights, and e^{3D}_q is the quadrature error that vanishes for quadrature rules of degree $\geq 2p-1$. Similarly, a 2D quadrature rule of arbitrary degree can approximate the integral of $\hat{\ell}^{2D}_{f,r} L^{2D}_{f,l}$ on $\mathbf{\Gamma}_f$ as follows

$$\int_{\mathbf{\Gamma}_f} \hat{\ell}^{2D}_{f,r} L^{2D}_{f,l} \; d\mathbf{\Gamma}_f = \sum_{s=1}^{N^{2D}_q} \omega_s \, \hat{\ell}^{2D}_{f,r}\left(\vartheta_s\right) L^{2D}_{f,l}\left(\vartheta_s\right) + e^{2D}_q, \tag{56}$$

where N^{2D}_q is the number of quadrature points, ϑ_s's are the point locations, ω_s's are the weights, and e^{2D}_q is the quadrature error that vanishes for quadrature rules of degree $\geq 2p$.

Upon substituting equations (55) and (56) into equations (53) and (54), one obtains

$$\left(\hat{\varepsilon}_{\mathbf{\Omega}_S}\right)_{i,m} = \sum_{j=1}^{N_p} \left(\hat{f}^D_{m,\,adv}\right)^j \sum_{n=1}^{N^{3D}_q} w_n \, \hat{\ell}^{3D}_j\left(\varsigma_n\right) L^{3D}_i\left(\varsigma_n\right) - \int_{\mathbf{\Omega}_S} \hat{f}_{m,\,adv}\left(\hat{u}^D\right) L^{3D}_i \; d\mathbf{\Omega}_S + E^{3D}_q, \tag{57}$$

$$\left(\hat{\varepsilon}_{\mathbf{\Gamma}_S}\right)_{f,l,m} = \sum_{r=1}^{N_{fp}} \left(\hat{f}^D_{m,f,\,dif}\right)^r \sum_{s=1}^{N^{2D}_q} \omega_s \, \hat{\ell}^{2D}_{f,r}\left(\vartheta_s\right) L^{2D}_{f,l}\left(\vartheta_s\right) - \int_{\mathbf{\Gamma}_f} \hat{f}_{m,\,dif}\left(\hat{u}^D_f, \hat{\mathbf{q}}^D_f\right) L^{2D}_{f,l} \; d\mathbf{\Gamma}_f + E^{2D}_q, \tag{58}$$

where

$$E^{3D}_q = \sum_{j=1}^{N_p} \left(\hat{f}^D_{m,\,adv}\right)^j e^{3D}_q, \qquad E^{2D}_q = \sum_{r=1}^{N_{fp}} \left(\hat{f}^D_{m,f,\,dif}\right)^r e^{2D}_q. \tag{59}$$

Now, if the quadrature rules are required to have a particular number of points, $N^{3D}_q = N_p$ and $N^{2D}_q = N_{fp}$, and the nodal solution points $\hat{\mathbf{x}}_i$ (or equivalently $\hat{\mathbf{x}}_j$) and nodal flux points $\hat{\mathbf{x}}_{f,l}$ (or equivalently $\hat{\mathbf{x}}_{f,r}$) are placed at the locations of the quadrature points ς_n and ϑ_s, one obtains

$$\left(\hat{\varepsilon}_{\mathbf{\Omega}_S}\right)_{i,m} = \sum_{j=1}^{N_p} \hat{f}_{m,\,adv}\left(\hat{u}^D\right) \Big|_{\varsigma_j} \sum_{n=1}^{N_p} w_n \, \delta_{jn} \, L^{3D}_i\left(\varsigma_n\right) - \int_{\mathbf{\Omega}_S} \hat{f}_{m,\,adv}\left(\hat{u}^D\right) L^{3D}_i \; d\mathbf{\Omega}_S + E^{3D}_q, \tag{60}$$

$$\left(\hat{\varepsilon}_{\mathbf{\Gamma}_S}\right)_{f,l,m} = \sum_{r=1}^{N_{fp}} \hat{f}_{m,\,dif}\left(\hat{u}^D_f, \hat{\mathbf{q}}^D_f\right) \Big|_{\vartheta_r} \sum_{s=1}^{N_{fp}} \omega_s \, \delta_{rs} \, L^{2D}_{f,l}\left(\vartheta_s\right) - \int_{\mathbf{\Gamma}_f} \hat{f}_{m,\,dif}\left(\hat{u}^D_f, \hat{\mathbf{q}}^D_f\right) L^{2D}_{f,l} \; d\mathbf{\Gamma}_f + E^{2D}_q, \tag{61}$$

or equivalently,

$$(\hat{\varepsilon}_{\mathbf{\Omega}_S})_{i,m} = \sum_{j=1}^{N_p} w_j \; \hat{f}_{m,\,adv}\left(\hat{u}^D\right)\Big|_{\varsigma_j} L_i^{3D}\left(\varsigma_j\right) - \int_{\mathbf{\Omega}_S} \hat{f}_{m,\,adv}\left(\hat{u}^D\right) L_i^{3D}\; d\mathbf{\Omega}_S + E_q^{3D}, \tag{62}$$

$$(\hat{\varepsilon}_{\mathbf{\Gamma}_S})_{f,l,m} = \sum_{r=1}^{N_{fp}} \omega_r \; \hat{f}_{m,\,dif}\left(\hat{u}_f^D, \hat{\mathbf{q}}_f^D\right)\Big|_{\vartheta_r} L_{f,l}^{2D}\left(\vartheta_r\right) - \int_{\mathbf{\Gamma}_f} \hat{f}_{m,\,dif}\left(\hat{u}_f^D, \hat{\mathbf{q}}_f^D\right) L_{f,l}^{2D}\, d\mathbf{\Gamma}_f + E_q^{2D}. \tag{63}$$

The sums in equations (62) and (63) act as numerical quadrature approximations of the integral terms in each of the equations, and evidently, for quadrature rules of sufficient strength, the integral terms and their numerical approximations will effectively cancel one another. In addition, (as mentioned previously) for quadrature rules of order $\geq 2p-1$ in 3D and $\geq 2p$ in 2D, the terms E_q^{3D} and E_q^{2D} will vanish. Thus, for quadrature rules of sufficient strength, $(\hat{\varepsilon}_{\mathbf{\Omega}_S})_{i,m}$ and $(\hat{\varepsilon}_{\mathbf{\Gamma}_S})_{f,l,m}$ approximately vanish, $\hat{\varepsilon}_{\mathbf{\Omega}_S}$ and $\hat{\varepsilon}_{\mathbf{\Gamma}_S}$ approximately vanish, and in turn $\varepsilon_{\mathbf{\Omega}_k}$ and $\varepsilon_{\mathbf{\Gamma}_k}$ approximately vanish. However, it is important to note that a quadrature rule of a very high degree maybe required for this to occur, and that there will frequently not be enough nodal solution points or nodal flux points to allow for this. Therefore, in practice, one should consider the act of placing the nodal solution points $\hat{\mathbf{x}}_i$ and nodal flux points $\hat{\mathbf{x}}_{f,l}$ at the locations of quadrature points as a procedure for reducing (but most likely not eliminating) aliasing errors. This procedure results in an effective compromise between the extremes of eliminating all aliasing errors via expensive L2 projections and creating large aliasing errors via inexpensive collocation projections that employ nodal solution and nodal flux point locations that differ from quadrature point locations.

Finding suitable quadrature rules on which to base the nodal solution and nodal flux point locations is a challenging task because of the following requirements:

1. The quadrature rules must have the correct numbers of points $N_q^{2D} = N_{fp}$ and $N_q^{3D} = N_p$ (as mentioned previously). In 2D, the quadrature rules must have N_{fp} points because the nodal set must be able to exactly represent a polynomial of degree p using $N_{fp} = 1$, 3, 6, 10, 15, or 21 points for $p = 0$ to $p = 5$. In 3D, the quadrature rules must have N_p points because the nodal set must be able to exactly represent a polynomial of degree p using $N_p = 1$, 4, 10, 20, 35, or 56 points for $p = 0$ to $p = 5$. This requirement is perhaps the most difficult to satisfy, as the vast majority of existing quadrature rules do not have the desired number of points.

2. The quadrature rules must be symmetric under affine transformations of the triangle unto itself and affine transformations of the tetrahedron unto itself. The locations of the nodal points must not introduce artificial asymmetries into the simulation of physical phenomena.

3. The quadrature rules must utilize points which reside within the interior or (at most) on the boundary of the triangle and tetrahedron.

4. The quadrature rules must result in a well-conditioned set of nodal basis functions. The associated nodal set must be well-conditioned in the sense that the Lebesgue constant Λ of the nodal basis functions must not be excessively large.

Recently, Shunn, Ham, and Williams[18,21] identified a set of quadrature rules for the triangle and tetrahedron that have the potential to satisfy these requirements. The quadrature rules are inspired by Sphere-Closed-Packed (SCP) lattice arrangements of points within the triangle and tetrahedron, (c.f. Figure (3) for examples of the SCP lattices on the equilateral triangle and tetrahedron). The quadrature rules and the degree of the highest polynomial that they exactly integrate are provided in Tables (1) and (2). The rules have the correct numbers of points (N_{fp} in 2D and N_p in 3D) and possess symmetric structures which mimic those of the SCP lattices in 2D and 3D. In addition, all quadrature points reside (strictly) within the interiors of the triangle and tetrahedron. However, the conditioning of these quadrature points has yet to be determined. Furthermore, the points have yet to be extensively used as nodal points on practical problems, thus it is unclear whether they have a substantial impact on the nonlinear aliasing errors of high-order nodal schemes such as the VCJH schemes.

In order to evaluate the quadrature points of Shunn, Ham, and Williams and to determine if they can be effectively utilized as nodal points, the authors will compare these points to the well-known 'α-optimized' points of Hesthaven

and Warburton[10], and Chen and Babushka[22]. The α-optimized sets of points were developed to be utilized as nodal points and are known to produce well conditioned interpolations and small Lebesgue constants. However, it is not yet clear whether these benefits outweigh their potential inability to act as good quadrature points and to attenuate aliasing error (by minimizing $\varepsilon_{\mathbf{\Omega}_k}$ and $\varepsilon_{\mathbf{\Gamma}_k}$). However, as discussed previously, the quadrature points of Shunn, Ham, and Williams may not necessarily represent a viable alternative, as they may produce ill-conditioned interpolations which may outweigh any potential benefits from their ability to reduce aliasing errors. In what follows, a thorough comparison of the aforementioned sets of nodal points is undertaken in order to obtain clarity regarding which points are more suitable for unsteady, nonlinear, flow problems.

IV. Conditioning of Nodal Sets

Calculations were performed in order to evaluate the conditioning of the nodal sets. In particular, the Lebesgue constant Λ was computed for each of the nodal sets in 2D and 3D. In 2D on a triangle, the Lebesgue constant takes the following form

$$\Lambda_{2D} = \sup_{\hat{x}} \sum_{i=1}^{N_{fp}} |\hat{\ell}_i^{2D}(\hat{x})|, \tag{64}$$

and, similarly, in 3D on a tetrahedron it takes the following form

$$\Lambda_{3D} = \sup_{\hat{x}} \sum_{i=1}^{N_p} |\hat{\ell}_i^{3D}(\hat{x})|. \tag{65}$$

The constant Λ can be interpreted as a measure of how far away $\hat{u}^D$ can venture from the best degree p polynomial approximation of the exact solution u. Alternatively, Λ can be interpreted as a condition number on the interpolation. In particular, if the vector of solution coefficients $\mathbf{U}_k$ is perturbed by a certain amount, then Λ characterizes how far the polynomial approximation can venture from its original form. Evidently, a smaller value of Λ is preferred.

In order to evaluate the conditioning of each of the point distributions, the Lebesgue constants were computed for $p = 1$ to $p = 5$ for the nodal points of Hesthaven and Warburton[10], Chen and Babushka[22], and Shunn, Ham, and Williams[18,21]. In addition, in order to establish a reference (or baseline), the Lebesgue constants were computed for nodal sets with points located at the centers of the 2D and 3D spheres in the 2D and 3D SCP lattices. The results are shown in Tables (3) and (4).

The best results are obtained by the α-optimized points from[10] and[22]. This is not unexpected, as the α-optimized points have been generated with the primary purpose of optimizing a single parameter 'α' (which controls the distribution of nodal points) with the purpose of minimizing Λ.

Note that the SCP-based quadrature points of Shunn, Ham, and Williams[18,21] produce values for Λ which are larger than those of the α-optimized points. However, the values of Λ are still seen to be much smaller than those associated with the naive choice of placing points at the centers of the spheres in the SCP lattices. Thus, the SCP-based quadrature points appear to produce values of Λ which are a reasonable compromise between those of the best and worst distributions of points that were tested.

V. Aliasing Errors of Nodal Sets

In order to evaluate the aliasing errors associated with the nodal sets, they were employed, in conjunction with the VCJH schemes, to solve the nonlinear Navier-Stokes (NS) equations. The NS equations in 3D can be written as follows

$$\frac{\partial U}{\partial t} + \nabla \cdot \mathbf{F}(U, \nabla U) = 0, \tag{66}$$

where U represents the conserved variables (which are scalars) and $\mathbf{F}$ represents the flux vector that is composed from inviscid and viscous parts: $\mathbf{F} = \mathbf{F}_{inv}(U) - \mathbf{F}_{visc}(U, \nabla U)$. In 3D, the conserved variables are defined as follows

$$U = \begin{Bmatrix} \rho \\ \rho u \\ \rho v \\ \rho w \\ E \end{Bmatrix}, \tag{67}$$

where $\rho = \rho(x, y, z, t)$ is the density, $u = u(x, y, z, t)$, $v = v(x, y, z, t)$, and $w = w(x, y, z, t)$ are the velocity components, $E = p/(\gamma - 1) + (1/2)\rho\left(u^2 + v^2 + w^2\right)$ is the total energy, $p = p(x, y, z, t)$ is the pressure, and γ is the ratio of specific heats. In addition, the inviscid and viscous fluxes in 3D can be defined in terms of their components along the x, y, and z coordinate directions, i.e. $\mathbf{F}_{inv} = (f_{inv}, g_{inv}, h_{inv})$ and $\mathbf{F}_{visc} = (f_{visc}, g_{visc}, h_{visc})$. Here, the inviscid flux components are defined such that

$$f_{inv} = \begin{Bmatrix} \rho u \\ \rho u^2 + p \\ \rho uv \\ \rho uw \\ u(E + p) \end{Bmatrix}, \qquad g_{inv} = \begin{Bmatrix} \rho v \\ \rho uv \\ \rho v^2 + p \\ \rho vw \\ v(E + p) \end{Bmatrix}, \qquad h_{inv} = \begin{Bmatrix} \rho w \\ \rho uw \\ \rho vw \\ \rho w^2 + p \\ w(E + p) \end{Bmatrix}, \tag{68}$$

and the viscous flux components are defined such that

$$f_{visc} = \mu \begin{Bmatrix} 0 \\ 2u_x + \lambda(u_x + v_y + w_z) \\ v_x + u_y \\ w_x + u_z \\ u[2u_x + \lambda(u_x + v_y + w_z)] + v(v_x + u_y) + w(w_x + u_z) + \frac{C_p}{Pr} T_x \end{Bmatrix},$$

$$g_{visc} = \mu \begin{Bmatrix} 0 \\ v_x + u_y \\ 2v_y + \lambda(u_x + v_y + w_z) \\ w_y + v_z \\ v[2v_y + \lambda(u_x + v_y + w_z)] + u(v_x + u_y) + w(w_y + v_z) + \frac{C_p}{Pr} T_y \end{Bmatrix},$$

$$h_{visc} = \mu \begin{Bmatrix} 0 \\ w_x + u_z \\ w_y + v_z \\ 2w_z + \lambda(u_x + v_y + w_z) \\ w[2w_z + \lambda(u_x + v_y + w_z)] + u(w_x + u_z) + v(w_y + v_z) + \frac{C_p}{Pr} T_z \end{Bmatrix}, \tag{69}$$

where μ is the dynamic viscosity, λ is the bulk viscosity coefficient, $T = p/(\rho R)$ is the temperature, R is the gas constant, C_p is the specific heat capacity at constant pressure, and Pr is the Prandtl number. It should be noted that the terms with subscripts x, y, and z in equation (69) signify first derivatives in x, y, and z (for example $T_z = \frac{\partial T}{\partial z}$).

Before proceeding further, it should be noted that equation (66) contains second derivatives of the conservative variables and can therefore be classified as a '2nd-order' system of PDEs. However, this system can easily be reformulated as a 1st-order system by eliminating ∇U from equation (66) and replacing it with the auxiliary variable denoted by Q as follows

$$\frac{\partial U}{\partial t} + \nabla \cdot \mathbf{F}(U, Q) = 0, \tag{70}$$

$$Q - \nabla U = 0. \tag{71}$$

This operation transforms equation (66) into a form that is more amenable to treatment by the VCJH schemes.

Experiments on equations (70) and (71) were performed with the VCJH schemes in conjunction with two 'representative' nodal sets: the nodal set based on the SCP-quadrature points of Shunn, Ham, and Williams[18,21], and the nodal set based on the α-optimized points of Hesthaven and Warburton[10]. Figure (4) illustrates the locations of the nodal solution points and nodal flux points for each nodal set, on the reference tetrahedron, for the case of $p = 3$.

A. Propagation of an Isentropic Vortex

In what follows, a VCJH scheme and the aforementioned nodal sets are employed to simulate the propagation of an inviscid, isentropic vortex. The propagation of an inviscid, isentropic vortex in a quiescent fluid is a well-known solution to the NS equations with $\mu = 0$ (i.e., the Euler equations). In this scenario, the vortex propagates indefinitely, and the exact solution can be straightforwardly computed from the initial conditions. In 3D, the exact solution of this problem takes the following form

$$\rho = \rho_0 \left(1 - \frac{\gamma - 1}{2}\Pi^2\right)^{\frac{1}{\gamma - 1}}, \tag{72}$$

$$\rho u = \rho \left(u_0 + r_x c_0 \, \Pi\right), \tag{73}$$

$$\rho v = \rho \left(v_0 + r_y c_0 \, \Pi\right), \tag{74}$$

$$\rho w = \rho \left(w_0 + r_z c_0 \, \Pi\right), \tag{75}$$

$$E = \frac{p_0}{\gamma - 1}\left(1 - \frac{\gamma - 1}{2}\Pi^2\right)^{\frac{\gamma}{\gamma - 1}} + \frac{\rho}{2}\left(u^2 + v^2 + w^2\right), \tag{76}$$

where

$$c_0 = \sqrt{\frac{\gamma p_0}{\rho_0}}, \tag{77}$$

$$\Pi = \Pi_{\max} \exp\left(\frac{1 - \left(\frac{|\mathbf{r}|}{r_0}\right)^2}{2}\right), \tag{78}$$

$$\mathbf{r} = \tilde{\mathbf{r}} \times \left(\mathbf{x} - \mathbf{x}_0 - \mathbf{u}_0 \, t\right), \tag{79}$$

and where c is the speed of sound, Π characterizes the strength of the vortex, r_0 is the radius of the vortex, and $\mathbf{r} = (r_x, r_y, r_z)$ and $\tilde{\mathbf{r}} = (\tilde{r}_x, \tilde{r}_y, \tilde{r}_z)$ are the orthogonal orientation vectors for the vortex. Here, it should be noted that all quantities subscripted by 0 denote values at initial time t_0.

Approximate solutions to the vortex propagation problem were sought on the cubic domain $\mathbf{\Omega} = [-10, 10] \times [-10, 10] \times [-10, 10]$. The cubic domain was discretized by forming $\tilde{N} \times \tilde{N} \times \tilde{N}$ regular hexahedral meshes and then splitting these meshes into grids with $N = 6\tilde{N}^3$ tetrahedron elements. In this manner, structured tetrahedral grids with $\tilde{N}$ = 16 and 32 were formed. Figure (5) shows the tetrahedral grid with $\tilde{N} = 16$.

Periodic boundary conditions were imposed on the boundaries of the cubic domain. The flow on the domain was initialized with $\rho_0 = 1$, $\gamma = 1.4$, $p_0 = \gamma^{-1}$, $\Pi_{\max} = 0.4$, $\mathbf{u}_0 = (0, 1, 0)$, $r_0 = 1$, $\tilde{\mathbf{r}}_0 = (0, 0, 1)$, and $\mathbf{x}_0 = (0, 0, 0)$. Figure (6) shows density contours of the initial flow.

The explicit 5-stage, 4th-order Runge-Kutta scheme of Carpenter and Kennedy[27] (denoted by RK54) was used to advance the approximate solution in time (starting from $t_0 = 0$) and, at each time-step, the inviscid and viscous numerical fluxes were computed using the Rusanov approach[28] and the LDG approach[29], respectively. Results were obtained on the aforementioned cubic domains with $\tilde{N} = 32$ and 16 for polynomial orders $p = 3$ and 4. In order to highlight the effects of aliasing errors, the approximate solutions were computed for long times (until time $t = 80$) using the VCJH scheme with $c = c_{dg}$ and $\kappa = \kappa_{dg}$, where it is important to note that the constants c and κ parameterize the VCJH scheme as described in[18]. This scheme is of particular interest because it is equivalent to the well-known, collocation-based, nodal DG scheme[18]. For this scheme, and for each set of nodal points, L2 errors in the energy E are shown in Table (5). In addition, contours of the density obtained with the α-optimized points for the case of $\tilde{N} = 32$ and $p = 3$ are shown in Figure (7). Note that the aliasing errors that frequently arose in each of the simulations are exemplified by the oscillations that distort the contours in Figure (7).

The data in Table (5) demonstrates that the simulations that utilize the quadrature points produce significantly less total error than the simulations that utilize the α-optimized points. It is reasonable to assume that these reductions in the total error are due to successful reductions in the aliasing error.

B. Flow Generated by a Time-Dependent Source Term

In what follows, a VCJH scheme and the aforementioned nodal sets are employed to solve the NS equations with a time-dependent source term S. In general, the term S is incorporated into the NS equations as follows

$$\frac{\partial U}{\partial t} + \nabla \cdot \mathbf{F}(U, Q) = S, \tag{80}$$

$$Q - \nabla U = 0. \tag{81}$$

It turns out that for certain choices of S, the NS equations have well-known exact solutions. In particular, if the source term is defined in 3D as follows

$$S = \begin{Bmatrix} s_1 \\ s_2 \\ s_3 \\ s_4 \\ s_5 \end{Bmatrix},$$

$$\begin{aligned}
s_1 &= (3k - \omega)\cos\left(k\left(x + y + z\right) - \omega t\right), \\
s_2 &= \frac{1}{2}\cos\left(k\left(x + y + z\right) - \omega t\right) \\
&\quad \left[\left(9 + 4a\left(\gamma - 1\right) - 3\gamma\right)k - 2\omega + 4\left(\gamma - 1\right)k\sin\left(k\left(x + y + z\right) - \omega t\right)\right], \\
s_3 &= \frac{1}{2}\cos\left(k\left(x + y + z\right) - \omega t\right) \\
&\quad \left[\left(9 + 4a\left(\gamma - 1\right) - 3\gamma\right)k - 2\omega + 4\left(\gamma - 1\right)k\sin\left(k\left(x + y + z\right) - \omega t\right)\right], \\
s_4 &= \frac{1}{2}\cos\left(k\left(x + y + z\right) - \omega t\right) \\
&\quad \left[\left(9 + 4a\left(\gamma - 1\right) - 3\gamma\right)k - 2\omega + 4\left(\gamma - 1\right)k\sin\left(k\left(x + y + z\right) - \omega t\right)\right], \\
s_5 &= \left(\frac{3\gamma k^2 \mu}{Pr}\right)\sin\left(k\left(x + y + z\right) - \omega t\right) + \frac{1}{2}\cos\left(k\left(x + y + z\right) - \omega t\right) \\
&\quad \left[3\left(3 - 3\gamma + 4a\gamma\right)k - 4a\omega + 4\left(3\gamma k - \omega\right)\sin\left(k\left(x + y + z\right) - \omega t\right)\right],
\end{aligned} \tag{82}$$

the following exact solution can be obtained

$$U = \begin{Bmatrix} \sin\left(k\left(x + y\right) - \omega t\right) + a \\ \sin\left(k\left(x + y\right) - \omega t\right) + a \\ \sin\left(k\left(x + y\right) - \omega t\right) + a \\ \sin\left(k\left(x + y\right) - \omega t\right) + a \\ \left(\sin\left(k\left(x + y\right) - \omega t\right) + a\right)^2 \end{Bmatrix}. \tag{83}$$

Approximate solutions to equations (80) and (81) were sought on a cubic domain $\mathbf{\Omega} = [-1, 1] \times [-1, 1] \times [-1, 1]$. The cubic domain was discretized by forming $\tilde{N} \times \tilde{N} \times \tilde{N}$ regular hexahedral meshes and then splitting these meshes into grids with $N = 6\tilde{N}^3$ tetrahedron elements. In this manner, structured tetrahedral grids with $\tilde{N}$ = 4, 6, 8, and 12 were formed.

Periodic boundary conditions were imposed on the boundaries of the cubic domain. At time $t = 0$, the flow on the domain was initialized with source term parameters $Pr = 0.72$, $\gamma = 1.4$, $k = \pi$, $\omega = \pi$, $a = 3.0$, and $\mu = 0.001$. Figure (8) shows density contours of the initial flow.

The solution was marched forward in time using the RK54 approach[27] and, at each time-step, the inviscid and viscous numerical fluxes were computed using the Rusanov approach[28] and the LDG approach[29], respectively. Results were obtained on the aforementioned cubic domains with $\tilde{N} = 12$, 8, 6, and 4 for polynomial orders $p = 2$, 3, 4, and 5. The approximate solutions were computed for long times (until time $t = 10$) using the VCJH scheme with $c = c_+$ and $\kappa = \kappa_+$. This scheme is of particular interest because (in some cases) it yields explicit time-step limits which are more than 2x larger than those of the collocation-based nodal DG scheme[18]. For this scheme, and for each set of

nodal points, L2 errors in the energy E are shown in Table (6). In addition, contours of the density obtained with the α-optimized points for the case of $N = 8$ and $p = 3$ are shown in Figure (9).

The results of the simulations are consistent with the results of the previous section, as the data in Table (6) demonstrates that the simulations that utilize the quadrature points produce less error than the simulations that utilize the α-optimized points. The reduction in error can be seen most notably for odd polynomial orders $p = 3$ and $p = 5$, where the error is reduced by roughly 25 – 50 percent. This suggests the existence of a diffusive phenomena that tends to dampen aliasing errors for even polynomial orders $p = 2$ and $p = 4$. More importantly, the tabulated data suggests that (regardless of whether the order is even or odd), the quadrature points are effective in reducing the aliasing errors, and in turn, reducing the total errors.

VI. Conclusion

It has been shown that placing nodal points at the locations of quadrature points reduces aliasing errors and results in moderately well-conditioned interpolations. These results has been demonstrated theoretically and empirically for a particular set of nodal points on tetrahedral elements. Specifically, a particular set of quadrature points has been shown to possess moderate values of the Lebesgue constants for polynomial orders $p = 1$ to $p = 5$. In addition, these points have been successfully employed to reduce aliasing errors in a number of experiments involving the nonlinear NS equations. It is hoped that the favorable performance of these points will result in their increasingly wide-spread utilization for nonlinear problems in the field of computational fluid dynamics.

Acknowledgments

The authors would like to acknowledge the support for this work provided by the Stanford Graduate Fellowships program, the National Science Foundation (NSF), and NVIDIA. The authors would also like to thank Peter E. Vincent, Patrice Castonguay, and Lee Shunn for engaging in many productive discussions that helped contribute to this work.

Tables

N_{fp}	Polynomial Integrated
1	1
3	2
6	4
10	5
15	7
21	8

Table 1. Strength of integration rules on the triangle due to Williams and Shunn[18].

N_p	Polynomial Integrated
1	1
4	2
10	3
20	5
35	6
56	8

Table 2. Strength of integration rules on the tetrahedron due to Shunn and Ham[21].

p	Λ_{2D} α[10]	Λ_{2D} SCP quadrature[18]	Λ_{2D} SCP
1	1.00	2.33	3.31
2	1.67	3.55	8.29
3	2.11	4.52	18.75
4	2.66	5.12	40.49
5	3.12	6.53	85.32

Table 3. Lebesgue constants for nodal sets on the reference triangle.

p	Λ_{3D} α[10]	Λ_{3D} α[22]	Λ_{3D} SCP quadrature[21]	Λ_{3D} SCP
1	1.00	1.00	2.85	4.67
2	2.00	2.00	4.39	15.10
3	2.93	2.93	6.14	41.76
4	4.07	4.11	8.28	106.26
5	5.32	5.62	29.59	256.84

Table 4. Lebesgue constants for nodal sets on the reference tetrahedron.

p	$\tilde{N}$	L_2 err. (quad-points)	L_2 err. (α-points)	% difference
3	32	2.24e-03	1.20e-02	438.19
4	16	6.04e-03	2.63e-02	335.11

Table 5. Comparison of errors produced by experiments with the quadrature points and the α-optimized points for the VCJH scheme with $c = c_{dg}$ and $\kappa = \kappa_{dg}$, for the problem involving inviscid, isentropic vortex propagation on tetrahedral grids, for the cases of $p = 3$ and $p = 4$.

p	$\tilde{N}$	L_2 err. (quad-points)	L_2 err. (α-points)	% difference
2	12	5.42e-01	5.45e-01	0.52
3	8	1.82e-01	2.28e-01	25.47
4	6	1.47e-01	1.51e-01	2.21
5	4	3.07e-01	4.63e-01	50.86

Table 6. Comparison of errors produced by experiments with the quadrature points and the α-optimized points for the VCJH scheme with $c = c_+$ and $\kappa = \kappa_+$, for the problem with flow driven by a time-dependent source term on tetrahedral grids, for the cases of $p = 2$ to $p = 5$.

Figures

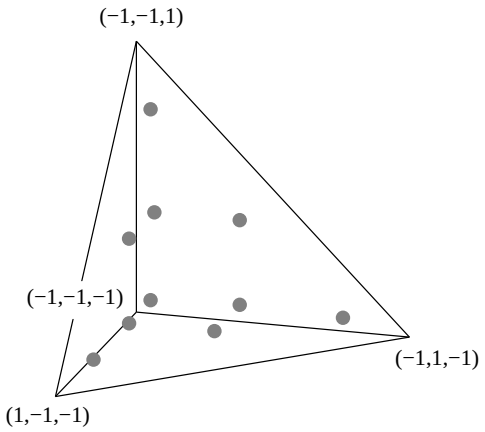

Figure 1. Example of the $N_p = 10$ solution point locations (denoted by circles) in the reference element for the case of $p = 2$.

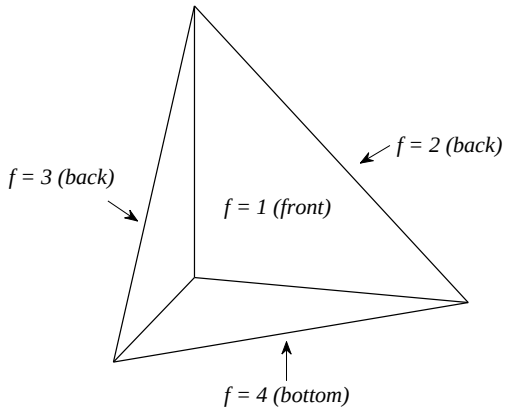

(a) Numbering convention on the faces of the reference element.

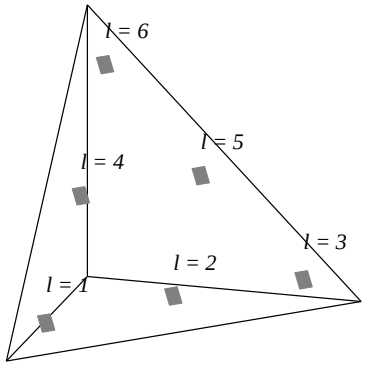

(b) Numbering convention for the flux points on a face of the reference element.

Figure 2. Example of the numbering convention for the flux points on the reference element for the case of $p = 2$. The flux points (denoted by squares) are shown for the face $f = 1$.

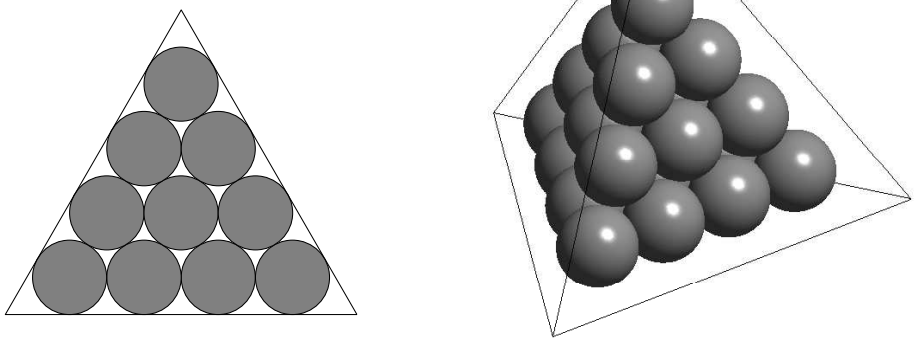

(a) $N_{fp} = 10$

(b) $N_p = 20$

Figure 3. Sphere closed packed (SCP) configurations with $N_{fp} = 10$ points on the triangle and $N_p = 20$ points on the tetrahedron.

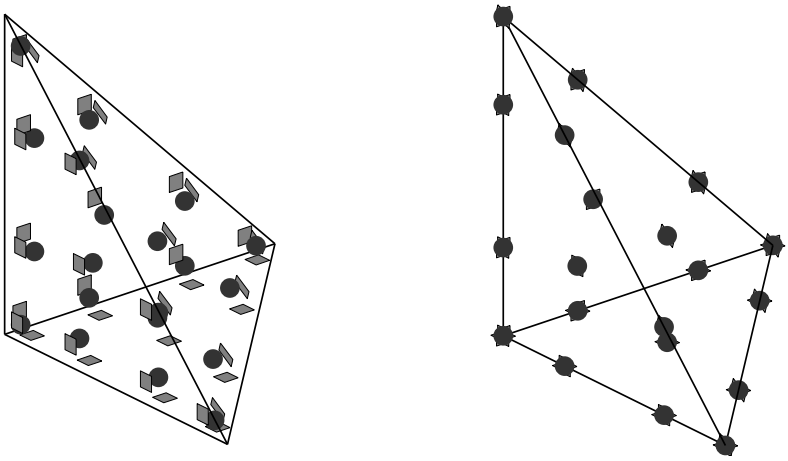

(a) Point arrangement based on quadrature points (b) Point arrangement based on α-optimized points

Figure 4. Placement of the solution points (circles) and flux points (squares) at the locations of the quadrature points and the α-optimized points for the case of $p = 3$.

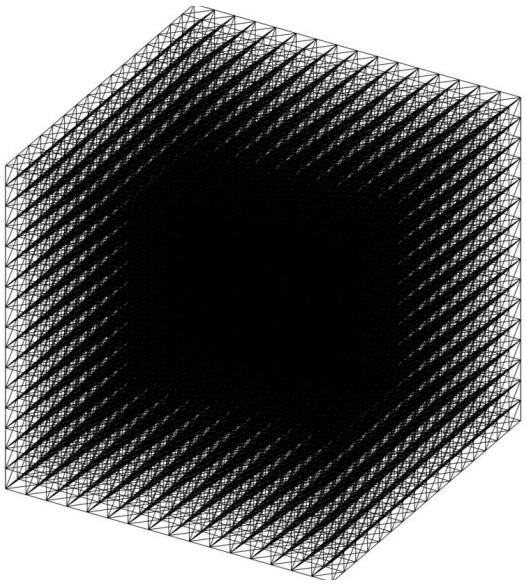

Figure 5. Structured tetrahedral grid for the case of $\tilde{N} = 16$.

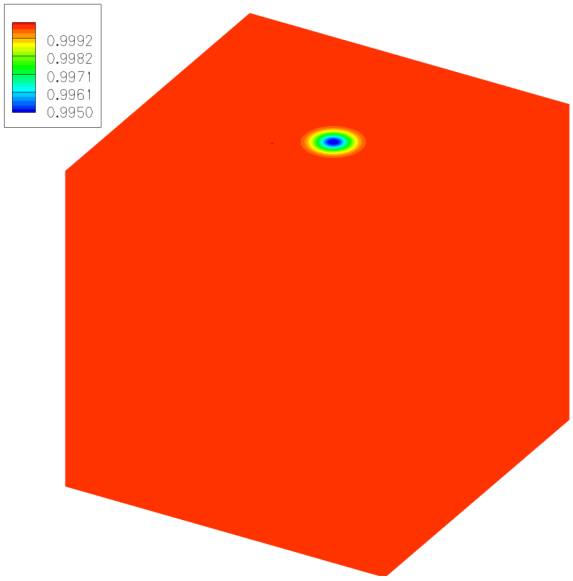

Figure 6. Contours of the density of the initial condition for the inviscid, isentropic vortex.

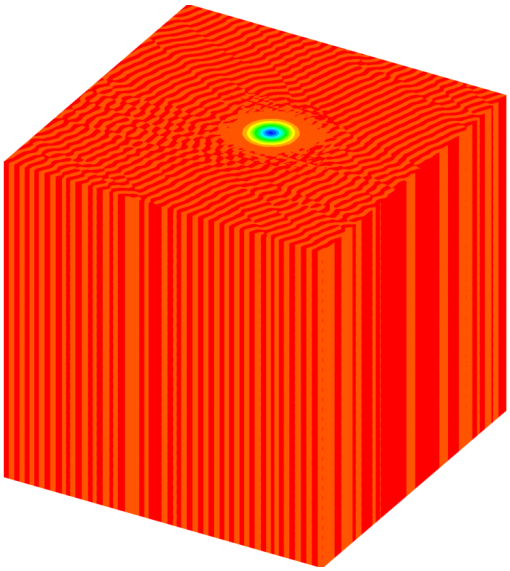

Figure 7. Contours of the density obtained via the VCJH scheme with $c = c_{dg}$, $\kappa = \kappa_{dg}$, and the solution and flux points placed at the locations of the α-optimized points, on the tetrahedral grid with $\tilde{N} = 32$ for the case of $p = 3$.

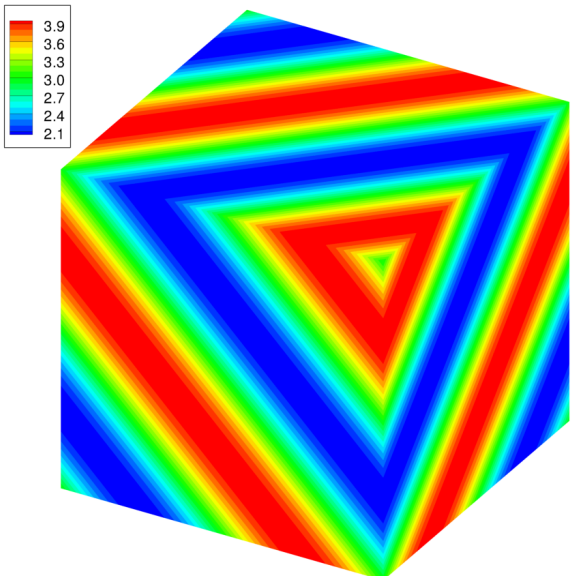

Figure 8. Contours of the density of the initial condition for the flow driven by a time-dependent forcing term.

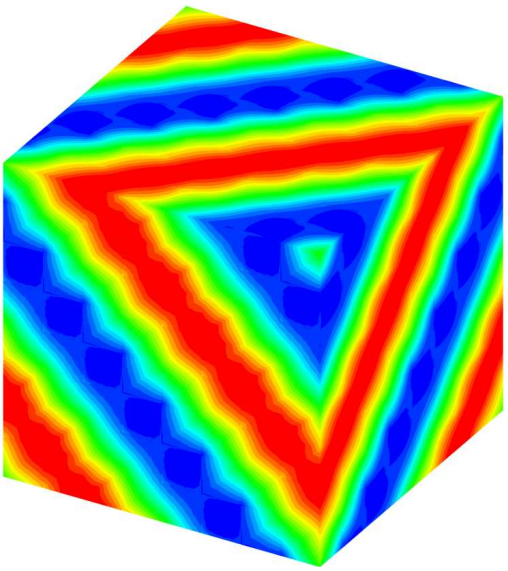

Figure 9. Contours of the density obtained via the VCJH scheme with $c = c_+$, $\kappa = \kappa_+$, and the solution and flux points placed at the locations of the α-optimized points, on the tetrahedral grid with $\tilde{N} = 8$ for the case of $p = 3$.

References

[1]Vincent, P. E. and Jameson, A., "Facilitating the Adoption of Unstructured High-Order Methods Amongst a Wider Community of Fluid Dynamicists," *Mathematical Modeling of Natural Phenomena*, Vol. 6, No. 3, 2011, pp. 97–140.

[2]Lomtev, I., Kirby, R. M., and Karniadakis, G. E., "A discontinuous Galerkin ALE method for compressible viscous flows in moving domains," *Journal of Computational Physics*, Vol. 155, No. 1, 1999, pp. 128–159.

[3]Persson, P.-O., Willis, D. J., and Peraire, J., "The numerical simulation of flapping wings at low Reynolds numbers," *48th AIAA Aerospace Sciences Meeting*, Orlando, FL, Jan. 4–7, 2010.

[4]Boelens, O., van der Ven, H., Oskam, B., and Hassan, A., "Boundary conforming discontinuous Galerkin finite element approach for rotorcraft simulations," *Journal of aircraft*, Vol. 39, No. 5, 2002, pp. 776–785.

[5]Bassi, F., Crivellini, A., Rebay, S., and Savini, M., "Discontinuous Galerkin solution of the Reynolds-averaged Navier-Stokes and k-[omega] turbulence model equations," *Computers & fluids*, Vol. 34, No. 4-5, 2005, pp. 507–540.

[6]Hartmann, R., Held, J., and Leicht, T., "Adjoint-based error estimation and adaptive mesh refinement for the RANS and k–ω turbulence model equations," *Journal of Computational Physics*, Vol. 230, No. 11, 2011, pp. 4268–4284.

[7]Cockburn, B., Hou, S., and Shu, C. W., "The Runge-Kutta local projection discontinuous Galerkin finite element method for conservation laws IV: the multidimensional case," *Mathematics of Computation*, Vol. 54, No. 190, 1990, pp. 545–581.

[8]Bassi, F. and Rebay, S., "High-order accurate discontinuous finite element solution of the 2D Euler equations," *Journal of Computational Physics*, Vol. 138, 1997, pp. 251–285.

[9]Bassi, F. and Rebay, S., "A High-Order Accurate Discontinuous Finite Element Method for the Numerical Solution of the Compressible Navier-Stokes Equations," *Journal of Computational Physics*, Vol. 131, No. 2, 1997, pp. 267–279.

[10]Hesthaven, J. S. and Warburton, T., *Nodal Discontinuous Galerkin Methods: Algorithms, Analysis, and Applications*, Springer Verlag, 2007.

[11]Kopriva, D. A. and Kolias, J. H., "A Conservative Staggered-Grid Chebyshev Multidomain Method for Compressible Flows," *Journal of Computational Physics*, Vol. 125, 1996, pp. 244–261.

[12]Liu, Y., Vinokur, M., and Wang, Z. J., "Spectral difference method for unstructured grids I: basic formulation," *Journal of Computational Physics*, Vol. 216, 2006, pp. 780–801.

[13]Huynh, H. T., "A Flux Reconstruction Approach to High-Order Schemes Including Discontinuous Galerkin Methods," *18th AIAA Computational Fluid Dynamics Conference*, Miami, FL, Jun. 25–28, 2007.

[14]Jameson, A., "A proof of the stability of the spectral difference method for all orders of accuracy," *Journal of Scientific Computing*, Vol. 45, No. 1, 2010, pp. 348–358.

[15]Vincent, P. E., Castonguay, P., and Jameson, A., "A new class of high-order energy stable flux reconstruction schemes," *Journal of Scientific Computing*, Vol. 47, No. 1, 2011, pp. 50–72.

[16]Castonguay, P., Vincent, P. E., and Jameson, A., "A new class of high-order energy stable flux reconstruction schemes for conservation laws on triangular grids," *Journal of Scientific Computing*, 2011, DOI: 10.1007/s10915-011-9505-3.

[17]Williams, D. M., Castonguay, P., Vincent, P. E., and Jameson, A., "Energy Stable Flux Reconstruction Schemes for Advection-Diffusion Problems on Triangles," *Journal of Computational Physics*, 2013, In Press.

[18]Williams, D. M., *Energy Stable High-Order Methods for Simulating Unsteady, Viscous, Compressible Flows on Unstructured Grids*, Ph.D. thesis, Stanford University, 2013.

[19]Jameson, A., Vincent, P. E., and Castonguay, P., "On the Non-Linear Stability of Flux Reconstruction Schemes," *Journal of Scientific Computing*, 2011, DOI: 10.1007/s10915-011-9490-6.

[20]Castonguay, P., Vincent, P. E., and Jameson, A., "Application of Energy Stable Flux Reconstruction Schemes for the Euler Equations," *49th AIAA Aerospace Sciences Meeting*, Orlando, FL, Jan. 4–7, 2011.

[21]Shunn, L. and Ham, F., "Symmetric quadrature rules for tetrahedra based on a cubic close-packed lattice arrangement," *Journal of Computational & Applied Mathematics*, Vol. 236, No. 17, 2012, pp. 4348–4364.

[22]Chen, Q. and Babuška, I., "Approximate optimal points for polynomial interpolation of real functions in an interval and in a triangle," *Computer Methods in Applied Mechanics and Engineering*, Vol. 128, No. 3, 1995, pp. 405–417.

[23]Viviand, H., "Conservative Forms of Gas Dynamic Equations," *La Recherche Aerospatiale*, Vol. 1, No. 1, 1974, pp. 65–66.

[24]Vinokur, M., "Conservation equations of gasdynamics in curvilinear coordinate systems," *Journal of Computational Physics*, Vol. 14, No. 2, 1974, pp. 105–125.

[25]Haga, T., Gao, H., and Wang, Z. J., "A High-Order Unifying Discontinuous Formulation for 3D Mixed Grids," *48th AIAA Aerospace Sciences Meeting*, Orlando, FL, Jan. 4–7, 2010.

[26]Haga, T., Gao, H., and Wang, Z. J., "A High-Order Unifying Discontinuous Formulation for the Navier-Stokes Equations on 3D Mixed Grids," *Mathematical Modelling of Natural Phenomena*, Vol. 6, No. 3, 2011, pp. 28–56.

[27]Carpenter, M. H. and Kennedy, C., "Fourth-order 2N-storage Runge-Kutta schemes," Tech. Rep. TM 109112, NASA, Langley Research Center, 1994.

[28]Rusanov, V. V., "Calculation of interaction of non-steady shock waves with obstacles," *Journal of Computational Math and Physics USSR*, Vol. 1, 1961, pp. 261–279.

[29]Cockburn, B. and Shu, C. W., "The local discontinuous Galerkin method for time-dependent convection-diffusion systems," *SIAM Journal on Numerical Analysis*, Vol. 35, No. 6, 1998, pp. 2440–2463.